JAST, Vol. 7, No. 1, pp 19–29


JAST
Journal of Aerospace Science and Technology

# Tomographic Reconstruction of the Ionospheric Electron Density in term of Wavelets

**Y. Amerian[1], M. M. Hossainali[2], B. Voosoghi[3], M.R. Ghaffari[4]**

*Ionospheric tomography is a method to investigate the ionospheric electron density in two or three dimensions. In this study, the function-based tomographic technique has been used for regional reconstruction of a 3D tomographic model of the ionospheric electron density using the GPS measurements of the Iranian Permanent GPS Network. Two-dimensional Haar wavelets and empirical orthogonal functions are used as base functions to model the horizontal and the vertical structure of the electron density, respectively. Sparseness of data and data gaps make ionospheric tomography an ill-posed inverse problem. The truncated singular value decomposition (TSVD) method is used to come up with solution. The data analysis results show that the latitudinal sections of the electron density in ionosphere obtained from the tomographic technique supports the expected time and height variations in the electron density. Moreover, these findings show that the height of maximum electron density is changed during the day. This confirms the efficiency of the developed multilayer model in comparison to the traditional single-layer ones. The relative error between the reconstructed electron density and the electron density obtained from ionosonde data varies between 5 to 35 percent. The difference between the reconstructed electron density (as well as the corresponding estimations of the IRI-2001 model) and the direct estimates of this quantity increases when the electron density reaches to its maximum value. Assuming that the ionosonde station in Tehran produces reliable results, this proves that the reconstructed image as well as the IRI-2001 model does not efficiently constraint the electron density during this period of time.*

## INTRODUCTION

During the last decade, GPS has become a common tool for analyzing the Earth's atmosphere. The ionosphere is that part of the atmosphere in which the number of free electrons is so high that it significantly affects the propagation of radiowaves. Radio signals are delayed by the ionosphere proportional to the inverse of their squared signal frequency. The fact that GPS and other GNSS systems broadcast signals on two or more frequencies can be used to measure the integrated ionospheric electron density TEC (Total Electron Content, electron density integrated along signal path from satellite to receiver on ground). The International GNSS Service (IGS) uses its dense global GNSS ground stations network to compute global ionospheric TEC maps on a routine basis (*e.g.* Hernandez-Pajares *et.al.*, 2009).With the development of regional and local permanent GPS networks, the spatial and temporal resolution of such studies has been considerably increased as compared to the traditional meteorological techniques. Determining TEC or electron density in this layer of atmosphere presents valuable information about ionosphere and its activities.

In the customary two dimensional modeling techniques, ionosphere is approximated by a thin spherical shell of free electrons located 250 to 450 Km above the

1. *Ph.D. Candidate, Faculty of Geodesy and Geomatics Eng., K.N. Toosi Univ. of Tech., Tehran, Iran, Email: amerian@dena.kntu.ac.ir.*
2. *Assitant Professor, Faculty of Geodesy and Geomatics Eng., K.N. Toosi Univ. of Tech., Tehran, Iran.*
3. *Associate Professor, Faculty of Geodesy and Geomatics Eng., K.N. Toosi Univ. of Tech., Tehran, Iran.*
4. *Formerly M.Sc. Student, Faculty of Geodesy and Geomatics Eng., K.N. Toosi Univ. of Tech., Tehran, Iran.*

earth's surface. The existing two dimensional methods of modeling the electron density can be classified to non-grid-based and grid-based techniques (El-Arini *et.al.* 1995). The former modeling techniques are based on the least squares estimation of a functional model for certain types of observables derived from the GPS carrier phase and code measurements. Polynomials and spherical harmonics are some of the base functions that are commonly in use (Walker 1989; Komjathy 1997; Schaer 1999; Coster *et.al.* 2003). In grid based modeling techniques, the spherical shell of free electrons is developed into a grid of rectangular elements. Special reconstruction algorithms are then used for estimating the electron density within the every element of the shell (El-Arini *et.al.* 1993 and 1994; Gao *et.al.* 1994; Skone 1998; Liao 2000; Liao and Gao 2001). In these models, the centroid height of the electron density profile (450 km) which is normally higher than the bulge height is generally used as a shell height. This assumption is not concurrent with real physical conditions of ionosphere, so an error is caused in ionospheric modeling. Neglecting the vertical gradient of the electron density is the main deficiency of the two dimensional modeling techniques. Specially, during high solar activity, this gradient and its impact on TEC is large (Komjathi 1997). Moreover, analyzing such variations to any accuracy is not possible due to dimensionality restriction of the model.

The application of the tomographic reconstruction to three dimensional modeling of the electron density using radio waves was for the first time proposed by Austen (Austen *et.al.*, 1988) and applied by Andreeva (Andreeva *et.al.* 1990). The remarkable results reported in (Andreeva *et.al.* 1990) encouraged the further analysis and development of this method (Raymund *et.al.* 1993; Foster et al. 1994; Mitchell 1997; Yin *et.al.* 2004; Yizengaw *et.al.* 2006). Methods of tomographic reconstruction are classified to function-based and voxel-based techniques. In the former approach, the electron density is developed into a set of analytical base functions which account for the horizontal and vertical variations of electron density within the ionosphere (Liao and Gao 2001). The system of simultaneous Equations to be solved for estimating electron density in this approach is badly conditioned, due to limited observability. Therefore, the application of regularization techniques for estimating a reliable solution is inevitable. In the latter method, the ionosphere is developed into a set of cubic elements whose electron density is estimated using special reconstruction algorithms (Hansen *et.al.* 1997; Colombo *et.al.* 1999; Hernandez-Pajares *et.al.*, 1999). The rank deficiency of the system of simultaneous Equations to be solved for estimating electron density in every cubic element is an inherent property of the voxel-based approach. In this paper, the function-based tomographic reconstruction is used for analyzing the three-dimensional structure of the electron density in Iran. The reproducibility of the electron density using the developed model is also checked using the ionosonde station in Tehran.

## OBSERVATIONS

Dual-frequency ground-based GPS receivers provides both the code $P_i$ and carrier phase $\Phi_i (i = 1, 2)$ observations on the $L1$ (1575.42 MHz) and $L2$ (1227.60 MHz) frequencies (Seeber 1993).

$L1$ frequency:

$$P_1 = \rho + c(dt - dT) + d_{orb} + d_{trop} + k_2 I + b_{p1} - B_{p1} + d_{mult/p1} + \epsilon(P_1) \quad (1)$$

$$\Phi_1 = \rho + c(dt - dT) + \lambda_1 N_1 + d_{orb} + d_{trop} - k_2 I + b_{\Phi 1} - B_{\Phi 1} + d_{mult/\Phi 1} + \epsilon(\Phi_1) \quad (2)$$

$L2$ frequency:

$$P_2 = \rho + c(dt - dT) + d_{orb} + d_{trop} + k_1 I + b_{p2} - B_{p2} + d_{mult/p2} + \epsilon(P_2) \quad (3)$$

$$\Phi_2 = \rho + c(dt - dT) + \lambda_2 N_2 + d_{orb} + d_{trop} - k_1 I + b_{\Phi 2} - B_{\Phi 2} + d_{mult/\Phi 2} + \epsilon(\Phi_2) \quad (4)$$

in which:

$$k_i = f_i^2/(f_1^2 - f_2^2), i = 1, 2; \quad (5)$$

$$I = 40.3\frac{TEC}{f_i^2} \quad (6)$$

where $\rho$ is the geometric range between the receiver and a satellite (m), $c$ is the speed of light (m/s), dt is the satellite clock error with respect to GPS time (s), dT is the receiver clock error with respect to GPS time (s), $d_{orb}$ is the satellite orbit error (m), $\lambda_i$ is the wavelength of the GPS signal on $L_i$ frequency, $N_i$ is the carrier phase integer ambiguity (cycle), $d_{trop}$ is the troposphere delay (m), $I$ is the ionospheric delay (m), $d_{mult}$ is the multipath effect (m), $b$ is the satellite hardware delay (m), $B$ is the receiver hardware delay (m) and $\epsilon$ is the measurement noise (m).

The parameter $TEC$ can be estimated using both the carrier phase and code measurements on the $L1$ and $L2$ frequencies. The combination of Equations (2) and (4) provide the following estimate of $TEC$ using the GPS carrier phase measurements ($TEC_\Phi$) (Liao and Gao 2001):

$$TEC_\Phi = \frac{f_1^2[(\lambda_1\Phi_1 - \lambda_2\Phi_2) - (\lambda_1 N_1 - \lambda_2 N_2) - b_i - b^p]}{40.3(\gamma - 1)} \quad (7)$$

Moreover, the combination of Equations (1) and (3) provide the following estimate of $TEC$ using the GPS code pseudo range measurements ($TEC_R$) (Liao and Gao 2001):

$$TEC_R = \frac{f_1^2[(P_1 - P_2) - B_i - B^p]}{40.3(1-\gamma)} \tag{8}$$

in which $\gamma$ is the square of the ratio of the $L1$ and $L2$ frequency:

$$\gamma = (\frac{f_1}{f_2})^2 = (\frac{77}{60})^2 \tag{9}$$

To come up with an absolute estimate of $TEC$ by Equation (7) requires a-priori estimates of the carrier phase biases $N_1$ and $N_2$. Since the ambiguities are unknown, $TEC_\Phi$ is, therefore, just a relative value of $TEC$. In contrast to $TEC_\Phi$, the estimation of $TEC_R$ does not require any a-priori information; therefore, $TEC_R$ provides an absolute estimate for $TEC$. Nevertheless, the accuracy of $TEC_\Phi$ is much higher than $TEC_R$. Differencing Equations (7) and (8) at an arbitrary epoch $n$ results in an estimate for the offset of $TEC_{R,n}$ and $TEC_{\Phi,n}$:

$$\Delta TEC_n = TEC_{R,n} - TEC_{\Phi,n} \tag{10}$$

If no cycle slip occurs during the measurements in $N$ successive epochs, the recursive Equation to calculate the mean $\Delta TEC_N$ at epoch $N$ is given below (Skone 1998):

$$\begin{aligned}\Delta TEC_N &= \frac{1}{N}\sum_{n=1}^{N}\Delta TEC_n = \frac{1}{N}\sum_{n=1}^{N}(TEC_{R,n} - TEC_{\Phi,n}) \\ &= \frac{1}{N}\left[\sum_{n=1}^{N-1}\Delta TEC_n + (TEC_{R,N} - TEC_{\Phi,N})\right]\end{aligned} \tag{11}$$

The smoothed absolute $TEC_{SM}$ at epoch $N$ is expressed as $TEC_{SM,N}$ and it can be calculated by (Liu 2004):

$$\begin{aligned}TEC_{SM,N} &= TEC_{\Phi,N} + \Delta TEC_N = \frac{f_1^2(\lambda_1\Phi_1 - \lambda_2\Phi_2)}{40.3(\gamma-1)} \\ &+ \frac{1}{N}\sum_{n=1}^{N}(\frac{f_1^2[(P_1 - P_2) + (\lambda_1\Phi_1 - \lambda_2\Phi_2)]}{40.3(1-\gamma)}) \\ &+ \frac{f_1^2(-B_i - B^p)}{40.3(1-\gamma)}\end{aligned} \tag{12}$$

The precision of $TEC_{SM,N}$ is better than $TEC_R$ and worse than $TEC_\Phi$. Therefore, this estimate of $TEC$ is known as smoothed $TEC$ (Skone 1998) where $TEC_{\Phi,N}$ is the relative total electron content derived from carrier phase measurements at epoch $N$. The accuracy of the smoothed $TEC_{SM,N}$ measurement is a function of the number of $N$. When the number of the smoothing epochs $N$ is larger, the smoothed results have higher accuracy.

## DEVELOPMENT OF A TOMOGRAPHIC MODEL

The total electron content ($TEC$) represents the total number of electrons in a column along the direction of a satellite (sv) to a receiver (rx) (Coster *et.al.* 2003). It can be expressed as:

$$\begin{aligned}TEC_{SM,N} &= \int_{rx}^{sv} N_e(\lambda,\phi,z)ds \\ &= \int_{rx}^{sv}[N_0(\lambda,\phi,z) + \delta N_e(\lambda,\phi,z)]ds\end{aligned} \tag{13}$$

in which, $TEC_{SM,N}$ is the smoothed total electron content at epoch $N$ obtained from Equation (12), $N_e(\lambda,\phi,z)$ denotes the ionospheric electron density function at the position $(\lambda,\phi,z)$. The ionospheric electron density function $N_e(\lambda,\phi,z)$ can be written as the sum of two parts $N_0(\lambda,\phi,z)$ and $\delta N_e(\lambda,\phi,z)$. The approximate value of the deterministic portion $N_0(\lambda,\phi,z)$ can be obtained from historical ionospheric electron density data or from the output of empirical ionosphere models and $\delta N_e(\lambda,\phi,z)$ is the corresponding correcting term which is sought in order to improve the accuracy of the empirical estimate $N_0(\lambda,\phi,z)$. The integral of the deterministic part of electron density function along the GPS signal path from satellite to receiver is defined as $TEC_0$:

$$TEC_0 = \int_{rx}^{sv} N_0(\lambda,\phi,z)ds \tag{14}$$

Thus Equation (13) can be written as:

$$TEC_{SM,N} = TEC_0 + \int_{rx}^{sv}\delta N_e(\lambda,\phi,z)ds \tag{15}$$

Defining the difference between total electron content measurement $TEC_{SM,N}$ and its approximate value $TEC_0$ as $\delta TEC$:

$$\delta TEC = TEC_{SM,N} - TEC_0 = \int_{rx}^{sv}\delta N_e(\lambda,\phi,z)ds \tag{16}$$

Inserting Equation (12) into Equation (16), it yields:

$$\delta TEC = \frac{f_1^2(\lambda_1\Phi_1 - \lambda_2\Phi_2)}{40.3(\gamma-1)} + \frac{1}{N}\sum_{n=1}^{N}\left(\frac{f_1^2[(P_1-P_2)+(\lambda_1\Phi_1-\lambda_2\Phi_2)]}{40.3(1-\gamma)}\right) + \frac{f_1^2(-B_i-B^p)}{40.3(1-\gamma)} - TEC_0 \quad (17)$$

Equation (16) is the mathematical model to be used for reconstructing the tomographic model. In function-based approach to tomographic reconstruction of the electron density, the correction term $\delta N_e(\lambda,\phi,z)$ is developed into a set of horizontal and vertical base functions. Two dimensional Haar wavelets $(H_n(\lambda,\phi))$ and empirical orthogonal functions (EOFs) $(Z_m(Z))$ have been used as the base functions for modeling the horizontal and vertical variation of the electron density respectively:

$$\delta N_e(\lambda,\phi,\mathrm{Z}) = \sum_{n=1}^{N}\sum_{m=1}^{M} a_{nm}H_n(\lambda,\phi)Z_m(Z) \quad (18)$$

Combining Equations (16) and (18), the mathematical model takes the following form:

$$\delta TEC = \int_{rx}^{sv}\sum_{n=1}^{N}\sum_{m=1}^{M} a_{nm}H_n(\lambda,\phi)Z_m(Z)\,ds \quad (19)$$

Equation (19) is the fundamental observation Equation for 3D modeling of the electron density using tomographic inversion technique through which the GPS derived total electron content ($TEC$) and the model coefficients describing the ionosphere are linked. The number of the unknown model parameters depends on the number of 2D Haar wavelets and EOFs are used as the basis function in the model.

**Horizontal base functions (Haar Wavelets)**

The intensity of the solar activity, which dominates the spatial and temporal distribution of the electron density, is not uniform in the course of time. Wavelets are an appropriate mathematical tool for analyzing such non-stationary signals (Boggess and Narcowich 2009). This paper tries to investigate the efficiency of one of the simplest forms of wavelets in reconstructing the horizontal variations of the electron density in ionosphere.

*One-Dimensional Haar Wavelet Basis Functions*

There are two functions that play a primary role in wavelet analysis: the scaling function *phi* and the wavelet $\psi$. These two functions generate a family of functions that can be used to break up or reconstruct a signal. To emphasize the "marriage" involved in building this "family", $\phi$ is sometimes called the "father wavelet" and $\psi$, the "mother wavelet" (Boggess and Narcowich 2009). The simplest wavelet analysis is based on the Haar Scaling Function, the graph of which is given in Figure 1.

This Haar scaling function is constant over the entire interval $[0,1)$ and zero elsewhere. Assuming that $V^0$ is the vector space of all these functions, the vector space containing functions with two constant pieces over the intervals $[0,0.5)$ and $[0.5,1)$ is called $V^1$. In this way, the vector space $V^j$ includes all piecewise-constant functions defined over the interval $[0,1)$ with constant pieces over each of $2^j$ equal subintervals. Every vector in $V^j$ is also contained in $V^{j+1}$ (Stollnitz *et.al.* 1995). Thus, spaces $V^j$, $j = 1,\ldots$ are a set of nested spaces; that is,

$$V^0 \subset V^1 \subset V^2 \subset \ldots \quad (20)$$

A simple basis for the vector space $V^j$ is given by the set of scaled and translated "box" functions:

$$\phi_k^j(x) := \phi(2^j x - k), \quad k = 0,\ldots,2^j-1 \quad \text{where} \quad \phi(x) := \begin{cases} 1 & \text{for } 0 \le x < 1 \\ 0 & \text{otherwise} \end{cases} \quad (21)$$

Figure 2 shows the four box functions forming a basis for $V^2$ (Stollnitz *et.al.* 1995).

If $W^j$ is the orthogonal complement of $V^j$ in $V^{j+1}$, then it consists of all functions in $V^{j+1}$ that are orthogonal to the elements of $V^j$ under the chosen inner product. Hence, the elements of the vector space $W^j$ provide a means for representing parts of a function in $V^{j+1}$ that cannot be represented in $V^j$. A collection of linearly independent functions $\psi_k^j(x)$ spanning $W^j$ are called wavelets. The wavelets corresponding to the

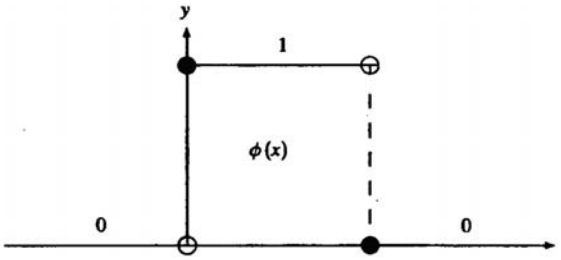


**Figure 1.** Haar scaling function (Boggess and Narcowich 2009)

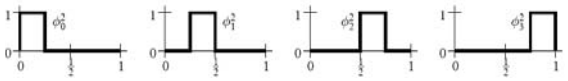

**Figure 2.** The box basis for $V^2$ (Stollnitz *et.al.* 1995)

box basis are known as the Haar wavelets given by:

$$\psi_k^j(x) := \psi(2^j x - k), \quad k = 0, ..., 2^j - 1$$

where

$$\psi(x) := \begin{cases} 1 & \text{for } 0 \le x < 0.5 \\ -1 & \text{for } 0.5 \le x < 1 \\ 0 & \text{otherwise} \end{cases} \tag{22}$$

Figure 3 shows the two Haar wavelets spanning $W^1$.

*Two-Dimensional Haar Wavelet Basis Functions*

For modeling the horizontal gradient of the electron density using the Haar wavelets as the basis functions, one dimensional Haar wavelets should be generalized into two dimensions. For this purpose, the existing methods can be classified into the standard and non-standard techniques. Figures 4 and 5 illustrate the steps to be taken in these techniques (Stollnitz *et.al.* 1995).

As these figures show, nonstandard Haar basis functions have square supports, while some standard basis functions have non-square supports. Depending on the desired application, standard basis functions may be preferred to the nonstandard ones or vice versa. No remarkable difference between the application of

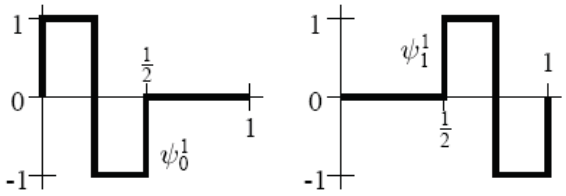


**Figure 3.** The Haar wavelet for $W^1$ (Stollnitz *et.al.* 1995).

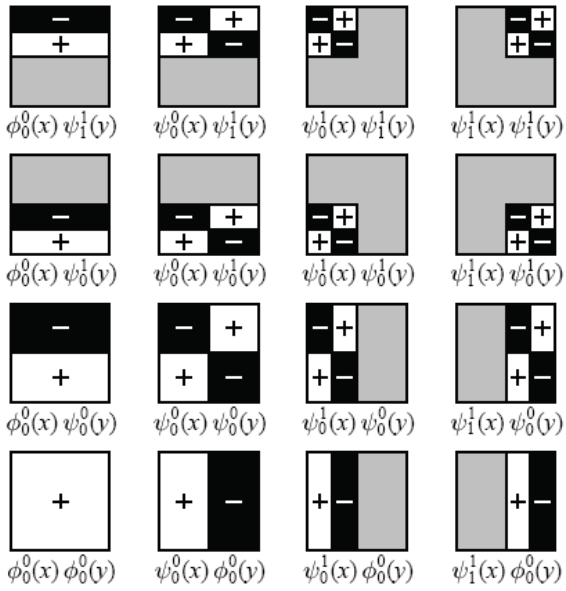


**Figure 4.** Standard construction of a two-dimensional Haar wavelet basis for $V^2$ (Stollnitz *et.al.* 1995).

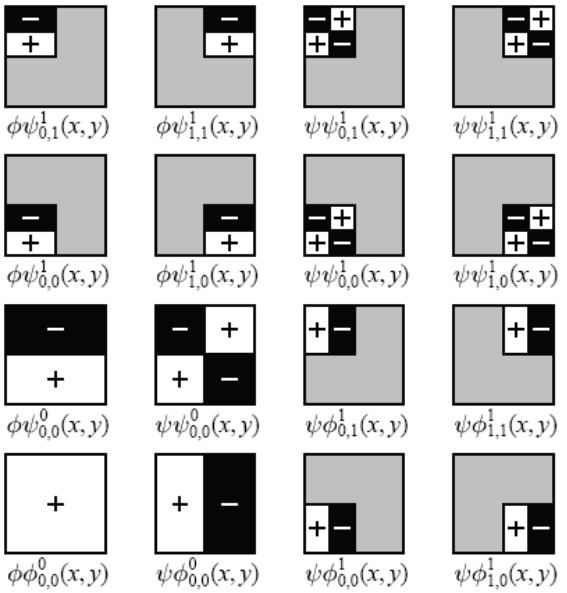


**Figure 5.** Nonstandard construction of a two-dimensional Haar wavelet basis for $V^2$ (Stollnitz *et.al.* 1995).

the nonstandard and standard functions is seen in the specific application of two-dimensional Haar wavelets in this research. To get an optimum estimate for the number of the required base functions, the relative error of the estimated electron density was compared with electron density measurements obtained from ionosonde. Using sixty four two-dimensional Haar basis functions provide the least relative error in the estimate values of the electron density.

**Estimating the Empirical Orthogonal Functions (EOFs)**

EOFs are derived from empirical data of the ionospheric electron density, which can be obtained from an empirical ionospheric model such as the International Reference Ionosphere (IRI) model or the direct measurements which are related to the electron density (such as ionosonde measurements) (Bilitza 2001). IRI models provide an initial estimate for the vertical profile of the electron density at any desired location in space and time. Having the samples of the density profile obtained at different times and heights, the matrix of electron density profile could be formed as:

$$N(t,h) = \begin{bmatrix} N(t_1,h_1) & N(t_1,h_2) & ... & N(t_1,h_N) \\ N(t_2,h_1) & N(t_2,h_2) & ... & N(t_2,h_N) \\ ... & ... & ... & ... \\ N(t_M,h_1) & N(t_M,h_2) & ... & N(t_M,h_N) \end{bmatrix} \tag{23}$$

in which, $N(t_i, h_j)$ is electron density in height $h_j (j = 1, 2, ..., N)$ and epoch $t_i (i = 1, 2, ..., M)$. The mean value of each column $(\bar{\mathbf{N}}(h_j))$ in this matrix provides an estimate for the mean value of the electron density

at a given height:

$$\overline{\mathbf{N}}(h_j) = \frac{1}{M}\sum_{m=1}^{M}\mathbf{N}(t_m, h_j)\ , \quad (j = 1, 2, .....N) \qquad (24)$$

The vertical variation of the electron density within the area of study (at an arbitrary epoch $t$) can be analyzed using the variation matrix $S$ below:

$$\mathbf{S} = \tilde{\mathbf{N}}^T(t,h)\tilde{\mathbf{N}}(t,h) \qquad (25)$$

in which, $\tilde{N}(t,h)$ is a matrix containing per column the difference between the corresponding elements of matrix $N$ from the mean value $\bar{N}(h_j)$ (Bjornsson and Venegas 1997). In mathematical statistics, the method of principal component analysis is used to explore the vertical variations that are inherent in Equation (25) (Jackson 2003). For this purpose, the principal (also known as empirical orthogonal) components of matrix S are firstly computed. Then, the contribution of every component to the total variations is analyzed.

If $x = [x_1, ..., x_p]^{\mathrm{T}}$ is a vector of random variables with $\sum$ variance-covariance matrix, the linear combinations $y_h = e_h^{\mathrm{T}}x$ is known as a principal component of this matrix where $e_h$ is the $h^{th}$ eigenvector of $\sum$. The corresponding eigenvalue $\lambda_h$ is the variance of this principal component (Johnson and Wichern 2002). Since the trace of the variance-covariance matrix of a random variable is equal to the sum of its eigenvalues, the ratio of every eigenvalue ($\lambda_i$) to this sum ($\sum_i \lambda_i$) is a measure for the contribution of the corresponding principal component to the total variation expressed by this summation. To come up with an optimum number of empirical orthogonal functions to account for the vertical variations of the electron density in the tomographic model, the contribution of the empirical orthogonal functions of matrix S has been computed and compared using the Equation $\left(\lambda_i / \sum_i \lambda_i\right) \times 100$. In this paper, matrices N and S have been created using the IRI-2001 empirical model.

The obtained results show that the first three principal components of matrix **S** include 99% of the total variations expressed by the sum of the eigenvalues. Therefore, the first three empirical orthogonal functions have been used for investigating the vertical variations of the electron density in this research. Figure 6 illustrates these empirical orthogonal functions.

## ESTIMATING THE MODEL PARAMETERS

Using the mathematical model (16), the simultaneous system of observation Equations can be written in the following form (Fremouw *et.al.* 1992 and 1994):

$$\mathbf{d} = \mathbf{Gm} + \mathbf{n} \qquad (26)$$

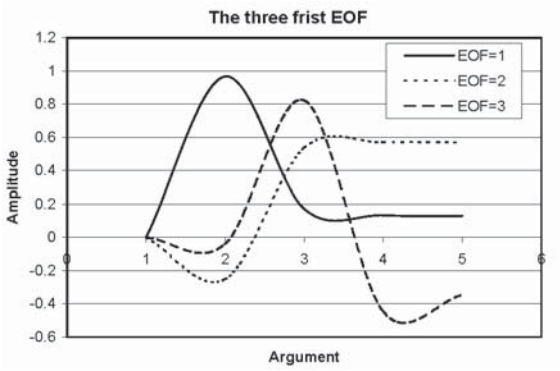


**Figure 6.** Vertical basis functions from IRI-2001 model.

in which **d** stands for the vector of observations (here $\delta TEC = TEC_{SM,N} - TEC_0$), **m** for the vector of model parameters (including unknown parameters $a_{nm}$), **G** for the design or coefficient matrix that describes the relations between observations and unknown parameters and n is the noise vector (observation random errors).

The integral Equation (19) is a Fredholm integral Equation of the first kind. It is mathematically proved that such integral Equations are improperly posed in the sense that the solution of their corresponding system of simultaneous Equations is not a continuous function of the input parameters (Hansen 1997). The spectral decomposition of the coefficient matrix can provide an immediate insight into the instability of solution for a system of simultaneous Equations. The asymptotic decay of the spectral values is an indication for the discontinuity of the solution because, for such a system of simultaneous Equations, the condition number is large and thereby perturbations of the input parameters are magnified on the outputs. The

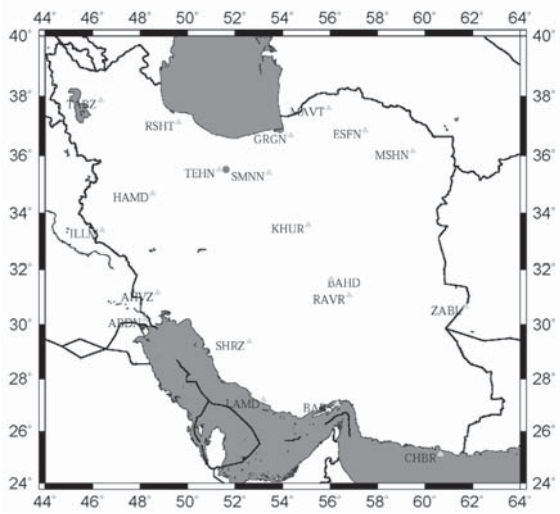


**Figure 7.** Distribution of the GPS stations in this study. Triangles in green illustrate the position of the GPS stations and the red circle indicates the position of the Tehran ionosonde station.

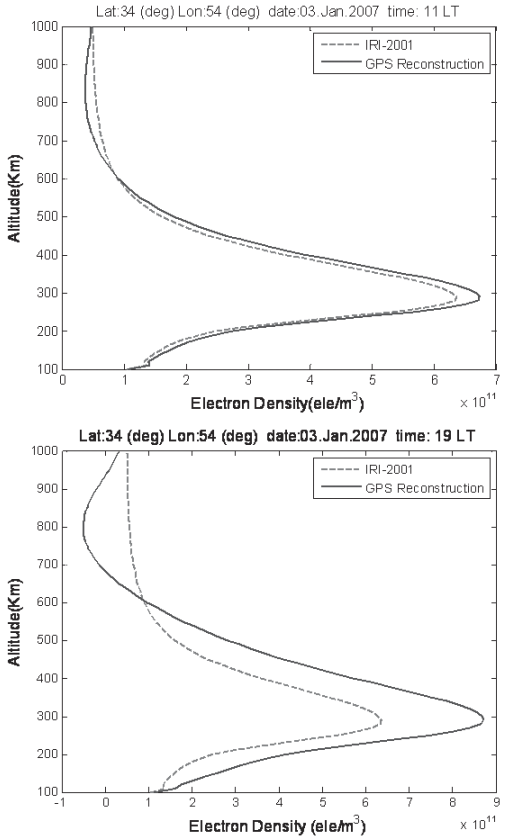


**Figure 8.** Variations of the electron's density (ele/m$^3$) for a specific position and time (2007.01.03).

following Equation provides an upper bound limit for the perturbations of the model parameters $\mathbf{m}$ as a function of the perturbations of input vector $\mathbf{d}$ (Jain *et.al.* 2003):

$$\frac{\|\tilde{m}-m\|}{\|m\|} \leq k\,(G)\,\frac{\left\|\tilde{d}-d\right\|}{\|d\|}, k\,(G)=\frac{\sigma_{\max}}{\sigma_{\min}} \tag{27}$$

where, $\tilde{\mathbf{m}}$ and $\tilde{\mathbf{d}}$ are the perturbed model parameters and input vector respectively and $k(\mathbf{G})$ is the condition number of the matrix $\mathbf{G}$, and $\sigma_{max}$ and $\sigma_{min}$ are the largest and smallest singular values of $\mathbf{G}$.

To come up with a stable solution for the model parameters, the application of regularization techniques is inevitable. In this paper the TSVD regularization technique has been used (Hansen 1987). According to the geometric theorem of singular value decomposition, the design matrix $\mathbf{G} \in R^{m\times n}$ , $m \geq n$ in Equation (26) can be expressed as follows (Watkins 2002):

$$\mathbf{G}=\mathbf{U}\mathbf{\Sigma}\mathbf{V}^T \tag{28}$$

in which, $\mathbf{U}=[\mathbf{u}_{.,1},\mathbf{u}_{.,2},...,\mathbf{u}_{.,m}] \in R^{m\times m}$ and $\mathbf{V}=[\mathbf{v}_{.,1},\mathbf{v}_{.,2},...,\mathbf{v}_{.,n}] \in R^{n\times n}$ are orthonormal matrices which include the left and the right singular vectors of matrix $\mathbf{G}$ respectively and $\mathbf{\Sigma}=diag(\sigma_1,\sigma_2,...,\sigma_n) \in R^{m\times n}$ is a diagonal matrix in which the diagonal elements are singular values of the design matrix. Based on this theorem, matrix $\mathbf{G}$ can be re-written as the sum of $n$ matrices of unit rank (Moler 2004):

$$\mathbf{G}=\mathbf{G}_1+\mathbf{G}_2+...+\mathbf{G}_n,\ \mathbf{G}_i=\sigma_i\mathbf{u}_i\mathbf{v}_i^T \tag{29}$$

In the function-based approach to the tomographic reconstruction: $r=rank(\mathbf{G})=n$ (*i.e.* there is no zero singular value in spectral decomposition of this matrix) but the singular values asymptotically decay to zero such that the change in solution is not a continuous function of the change in the input parameters. Therefore, the problem is improperly posed and the application of regularization techniques to achieve a stable solution is inevitable. Similar to the other regularization techniques, the idea of TSVD is to replace the ill-conditioned problem by a more stable one that is directly related to the main problem but is less sensitive to the input perturbations. For this purpose, matrix $\mathbf{G}$ is replaced by $\mathbf{G}_k$ which is given by:

$$\mathbf{G}_k=\mathbf{U}\mathbf{\Sigma}_k\mathbf{V}^T,$$
$$\mathbf{\Sigma}_k=diag(\sigma_1,\sigma_2,...,\sigma_k,0,...,0) \in R^{m\times n}, \quad k<n \tag{30}$$

$\mathbf{G}_k$ approximates $\mathbf{G}$ by substituting the last $n-k$ singular values by zero. Through this process the conditioning of the system improves to $k\,(G_k)=\frac{\sigma_1}{\sigma_k}$. The central point in any regularization technique is to find a compromise between the resolution of regularized solution and the stability of the system. This is achieved by finding an optimum regularization parameter. With regard to the truncated singular value decomposition, the number of singular values to reject plays the role of regularization parameter. The SVD is successfully truncated at $k$, if there is a well-determined gap between the singular values $\sigma_k$ and $\sigma_{k+1}$ (Hansen 1987).

## NUMERICAL RESULTS

To reconstruct 3D-images of electron density over Iran, observations of 22 GPS sites from the Iranian Permanent GPS Network (IPGN), equipped with dual-frequency GPS receivers, were used. Observations from January 03, 2007 have been used for this purpose. Figure 7 illustrates the spatial distribution of these stations. This figure also shows the position of the only ionosonde station in Iran, which is located in the Institute of Geophysics of the University of Tehran. Ionosondes provide direct measurements of the ionospheric electron density. Thus, the Tehran ionosonde measurements (Lat.=35.7382$^o$, Long.=51.3851$^o$) were used to validate the electron density values computed

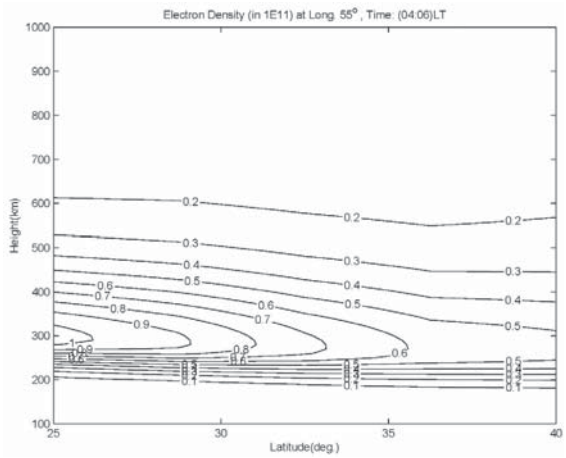


**Figure 9.** Latitudinal section of electron density (ele/m$^3$) at 04:06 LT on January 03, 2007.

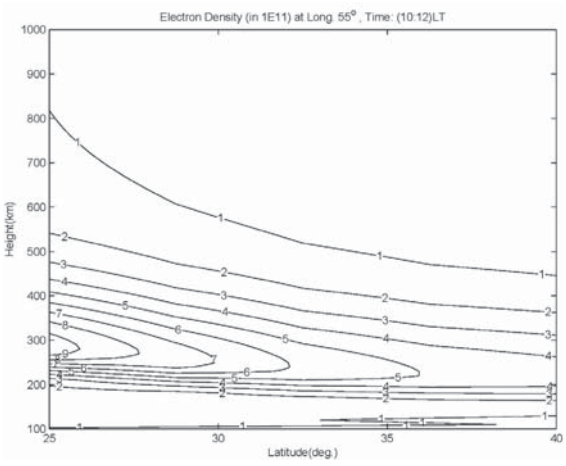


**Figure 10.** Latitudinal section of electron density (ele/m$^3$) at 10:12 LT on January 03, 2007.

with the tomographic model. Since the direct measurements at the ionosonde station are in a different epoch corresponding to a different height, profiles of the electron density cannot be derived from individual measurement epochs.

Figure 8 illustrates the GPS reconstructed profiles of the electron density obtained from the tomographic technique and those obtained from the IRI-2001 model for two different epochs.

Figures 9, 10, 11 and 12 show latitudinal cross-sections of ionospheric electron density obtained from the tomographic techniques used in this study. It can be seen that the maximum electron density appears at 10h – 12h local time and at an altitude of 300 – 400 km above the earth surface. This corresponds to the expected daily behaviour of electron density. Contrary to the 2D (single layer) models (El-Arini *et.al.*, 1993 and 1994), in which a constant (in time and space) shell height coinciding with a mean electron density profile centroid height is assumed, our tomographic approach accounts for time and space variations of maximum electron density height. This observation is confirmed by the direct measurements. Figure 13 shows the horizontal variations of the electron density in Iran suggested by the developed tomographic image (in $10^{10}$ m$^{-3}$).

In Table 1, reconstructed electron density and its estimate from the direct measurements of the ionosonde station (in $10^{11}$ m$^{-3}$) are compared. Figure 14 provides a point-wise comparison between the reconstructed electron density, the estimation of this quantity proposed for by IRI-2001model and the one obtained from the ionosonde data.

## CONCLUSIONS

In this study, the function-based tomographic technique has been used for regional reconstruction of a 3D tomographic model of the ionospheric electron density using the GPS measurements of the Iranian Permanent GPS Network. 2D Haar wavelets and em-

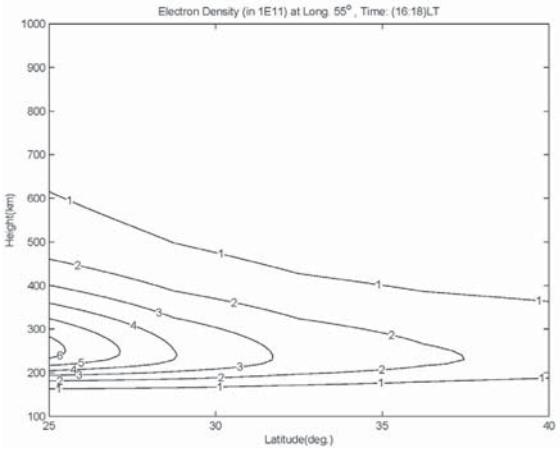


**Figure 11.** Latitudinal section of electron density (ele/m$^3$) at 16:18 LT on January 03, 2007.

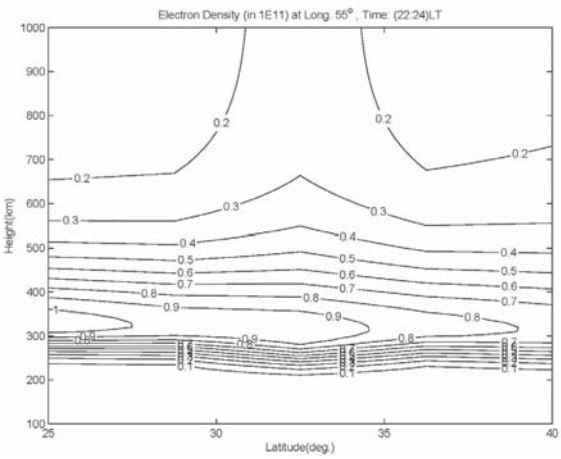


**Figure 12.** Latitudinal section of electron density (ele/m$^3$) at 22:24 LT on January 03, 2007.

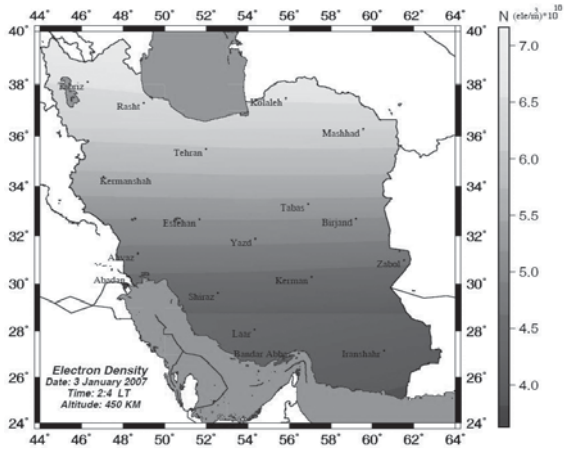


**Figure 13.** Electron Density (in $10^{10}$ $m^{-3}$) at 02:04 LT on January 03, 2007.

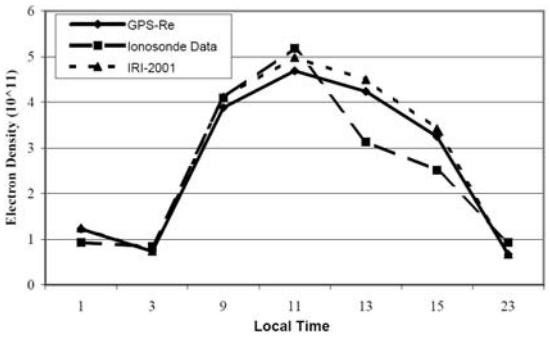


**Figure 14.** Reconstructed electron density and electron density from ionosonde on January 03, 2007.

pirical orthogonal functions are used as base functions to model the horizontal and the vertical content of the electron density, respectively. The data analysis results show that the latitudinal sections of the electron density in ionosphere obtained from the tomographic technique support the expected time and height variations in the electron density. Moreover, these findings show that the height of maximum electron density is changed during the day. This confirms the efficiency of the developed multilayer model in comparison to the traditional single-layer ones. The relative error between the reconstructed electron density and the electron density obtained from ionosonde data changes from 5 to 35 percent. According to Figure 14, the difference between the reconstructed electron density (as well as the corresponding estimations of the IRI-2001 model) and the direct estimates of this quantity increases when the electron density reaches to its maximum value. Assuming that the ionosonde station in Tehran produces reliable results, this proves that the reconstructed image as well as the IRI-2001 model does not efficiently constraint the electron density during this period of time.

## ACKNOWLEDGMENTS

Authors would like to thank the NCC (National Cartographic Center of Iran) for providing GPS data and the Institute of Geophysics of the University of Tehran for providing ionosonde data. This paper benefited from constructive reviews of anonymous reviewers.

## REFERENCES

1. Andreeva E.S, Galinov A.V, Kunitsyn V.E, Mel'nichenko Y.A, Tereshchenko E.D, Filimonov M.A, Chernykov S.M, "Radiotomographic Reconstructions of Ionization Dip in the Plasma Near the Earth", *Journal of Experimental and Theoretical Physics Letter*, **52**, PP 145-148(1990).
2. Austen J.R., Franke S.J., Liu C.H., "Ionospheric Imaging Computerized Tomography", *Radio Sci.*, **23**, PP 299-307(1988).
3. Bilitza D., "International Reference Ionosphere 2000", *Radio Science*, **36**(2), PP 261-275(2001).
4. Bjornsson H., Venegas S.A., "A Manual for EOF and SVD Analyses of Climate Data", Department of Atmospheric and Oceanic Sciences and Center for Climate and Global Change Research, McGill University, (1997).
5. Boggess A., Narcowich F.J., *A First Course in Wavelets with Fourier Analysis*, John Wiley & Sons, (2009).
6. Colombo O.L., Hernandez-Pajares M., Juan J.M., Sanz J., Talaya J. , "Resolving Carrier-Phase Ambiguities On The Fly, At More Than 100 km From Nearest Reference Site, With The Help Of Ionospheric

**Table 1.** Reconstructed electron density and electron density from the ionosonde measurement on January 03, 2007 (in $10^{11}$ $m^3$).

| Time | Altitude(km) | Reconstructed Electron Density | Direct Measurements | Relative Error (%) |
|---|---|---|---|---|
| 1 | 278 | 1.223 | 0.9243 | -32.256 |
| 3 | 233 | 0.7367 | 0.8382 | +12.112 |
| 9 | 219 | 3.884 | 4.1 | +5.288 |
| 11 | 226 | 4.689 | 5.192 | +9.685 |
| 13 | 211 | 4.240 | 3.138 | -35.116 |
| 15 | 198 | 3.252 | 2.512 | -29.48 |
| 23 | 281 | 0.6674 | 0.9378 | +28.824 |

Tomography", Proceeding of ION GPS-99, Nashville, USA, (1999).

7. Coster A.J., Foster J., Erickson P., "Monitoring the Ionosphere with GPS", *Space Weather, GPS World*, **14(5)**, PP 42-49(2003).
8. El-Arini M.B., Hegarty C.J., Fernow J.P., Klobuchar J.A., "Development of an Error Budget for a GPS Wide-Area Augmentation System (WAAS)", *Proceeding of the Institute of Navigation NTM-94*, San Diego, CA, (1994).
9. El-Arini M.B., O[Donnell P.A., Kellam P., Klobuchar J.A., Wisser T.C., Doherty P.H. , "The FAA Wide Area Differential GPS (WADGPS) Static Ionosphere Experiment", *Proceeding of the Institute of Navigation NTM-93*, San Francisco, CA, (1993).
10. El-Arini M.B., Conker R.S., Albertson T.W., Reagan J.K., Klobuchar J.A., Doherty P.H., "Comparison of Real-Time Ionosphere Algorithms for a GPS Wide-Area Augmentation System (WAAS)", *Journal of The Institute of Navigation*, **41(4)**, PP 393-413(1995).
11. Foster J.C., Buonsanto M.J., Klobuchar J.A., Holt J.M., Fougere P., Pakula W.A., Raymund T.D., Kunitsyn V.E., Andreeva E.S., Tereschenko E.D., Kudukon B.Z., "Russian American Tomography Experiment", *International Journal of Imaging System and Technology*, **5**, PP 148-159(1994).
12. Fremouw E.J., Secan J.A., Bussey R.M., Howe B.M. , "A Status Report on Applying Discrete Inverse Theory to Ionospheric Tomography", *Int. J. Imaging Syst. Technol.*, **5**, PP 97-105(1994).
13. Fremouw E.J., Secan J.A., Howe B.M., "Application of Stochastic Inverse Theory to Ionospheric tomography", *Radio Sci.*, **27**, PP 721-732(1992).
14. Gao Y., Heroux P., Kouba J., "Estimation of GPS Receiver and Satellite L1/L2 Signal Delay Biases Using Data from CACS, Processing of KIS-94", Banff, Canada, (1994).
15. Hansen A.J., Walter T., Enge P., "Ionospheric Correction Using Tomography", *Proceeding of 10th International Technical Meeting of the Satellite Division of the Institute of Navigation, ION GPS-97*, PP 249-260(1997).
16. Hansen P.C., "The Truncated SVD as a Method for Regularization", *BIT*, **27**, PP 534-553(1987).
17. Hansen P.C., "Rank-Deficient and Discrete Ill-Posed Problems: Numerical Aspects of Linear Inversion", *SIAM Monographs on Mathematical Modeling and Computation*, (1997).
18. Hernandez-Pajares M., Juan J.M., Sanz J., Orus-Perez R., Garcia-Rigo A., Feltens J., Komjathy A., Schaer S.C. and Krankowski A., "The IGS VTEC Maps: a Reliable Source of Ionospheric Information Since 1998", *J. Geod*, (2009).
19. Hernandez-Pajares M., Juan J.M. and Sanz J., "New Approaches in Global Ionospheric Determination Using Ground GPS Data", *Journal of Atmospheric and Solar Terrestrial Physics*, **61**, PP 1237 - 1247(1999).
20. Jain M.K., Iyengar S.R.K., Jain R.K. , *Numerical Methods for Scientific and Engineering Computation*, New Age International (P) Limited, (2003).
21. Jackson J.E., *A Users' Guide to Principal Components*, Wiley & Sons Inc., (2003).
22. Johnson R.A., Wichern D.W., *Applied Multivariate Statistical Analysis*, Prentice Hall, Upper Saddle River, (2002).
23. Komjathy A., "Global Ionospheric Total Electron Content Mapping Using the Global Positioning System", Ph.D. Dissertation, Department of Geodesy and Geomatics Engineering, Technical Report No. 188, University of New Brunswick, Canada, (1997).
24. Liao X., "Carrier Phase Based Ionosphere Recovery over a Regional Area GPS Network", *UCGE Reports, Number 20143*, The University of Calgary, Calgary, Alberta, Canada, (2000).
25. Liao X., Gao Y., "High-Precision Ionosphere TEC Recovery Using a Regional-Area GPS Network", *Navigation*, **48(2)**, PP 101-111(2001).
26. Liu Z., "Ionosphere Tomographic Modeling and Applications Using Global Positioning System (GPS) Measurments", *UCGE Reports, Number 20198*, University of CALGARY, (2004).
27. Mitchell C.N., Kersley L., Heaton J.A.T., Pryse S.E., "Determination of the Vertical Electron-Density Profile in Ionospheric Tomography: Experimental Results", *Annales Geophysicae*, **15**, PP 747-752(1997).
28. Moler C., "Numerical Computing with Matlab", (2004).
29. Raymund T.D., Pryse S.E., Kersley L., Heaton J.A.T. , "Tomographic Reconstruction of Ionospheric Electron Density with European Incoherent Scatter Radar Verification Methods", *Radio Science*, **28**, PP 811-818(1993).
30. Schaer S., "Mapping and Predicting the Earth's Ionosphere Using the Global Positioning System", Ph.D. Dissertation, Astronomical Institute, University of Berne, Switzerland, (1999).
31. Seeber G., "Satellite Geodesy: Foundations, Methods and Application", *Walter de Gruyter, Berlin and New York*, (1993).
32. Skone S., "Wide Area Ionosphere Grid Modeling in the Auroral Region", *UCGE Reports Number 20123*, Ph.D. Thesis, The University of Calgary, Calgary, Alberta, Canada, (1998).
33. Stollnitz E.J., DeRose T.D., Salesin D.H., "Wavelets for Computer Graphics: A Primer, Part 1", *IEEE Computer Graphics and Applications*, **15(3)**, PP 76-84(1995).
34. Walker J.K., "Spherical Cap Harmonic Modeling of High Latitude Magnetic Activity and Equivalent Sources with Sparse Observations", *Journal of Atmospheric and Terrestrial Physics*, **51(2)**, PP 67-80(1989).

35. Watkins D.S., *Fundamentals of Matrix Computations*, John Wiley & Sons, (2002).
36. Yin P., Mitchell C.N., Spencer P.S.J., Foster J.C., "Ionospheric Electron Concentration Imaging Using GPS over the USA During the Storm of July 2000", *Geophysical Research Letters, L12806*, (2004).
37. Yizengaw E., Moldwina M.B., Dysonb P.L., Essexb E.A., "Using Tomography of GPS TEC to Routinely Determine Ionospheric Average Electron Density Profile", Institute of Geophysics and Planetary Physics, University of California Los Angeles, USA, (2006).